Microscopy, 2022, **71(S1)**, i3–i14
DOI: https://doi.org/10.1093/jmicro/dfab049
Supplement Paper

MICROSCOPY

Recent progress and future perspective of electron cryomicroscopy for structural life sciences

Keiichi Namba[1,2,3,*] and Fumiaki Makino[1,4]

[1]Graduate School of Frontier Biosciences, Osaka University, 1-3 Yamadaoka, Suita, Osaka 565-0871, Japan
[2]RIKEN Center for Biosystems Dynamics Research & SPring-8 Center, 1-3 Yamadaoka, Suita, Osaka 565-0871, Japan
[3]JEOL YOKOGUSHI Research Alliance Laboratories, Osaka University, 1-3 Yamadaoka, Suita, Osaka 565-0871, Japan
[4]JEOL Ltd, 3-2-1 Musashino, Akishima, Tokyo 196-8558, Japan
[*]To whom correspondence should be addressed. E-mail: keiichi@fbs.osaka-u.ac.jp

Abstract

The three-dimensional structure of biological macromolecules, such as proteins and nucleic acids, and their complexes is the fundamental information not only for life sciences but also for medical sciences and drug design. Electron cryomicroscopy has become an extremely powerful tool for high-resolution structural analysis of biological macromolecules, not just in addition to X-ray crystallography and nuclear magnetic resonance sepectroscopy (NMR) that have been used as the basic techniques in structural biology. By the development of hardware and software, such as transmission electron cryomicroscopes with highly stable and controllable electron optics, cold field emission gun and energy filter, complementary metal oxide semiconductor (CMOS)-based direct electron detectors with high frame rate and high sensitivity, high-speed computers and software programs for image analysis, electron cryomicroscopy now allows structure determination of biological macromolecules at atomic levels within a few days even from a drop of solution sample with an amount as small as a few micrograms. How can the structures of macromolecules be imaged and analyzed at atomic level resolution in their native states despite their high sensitivity to radiation damage at a relatively low level of electron irradiation? We describe recent progress and future perspective of electron cryomicroscopy for structural life sciences.

Key words: electron microscopy, single-particle image analysis, structural biology, macromolecular structure, high-throughput data collection, high-resolution structure

Introduction

The basic mechanisms that drive and support complex biological activities are highly shared by diverse organisms, from microorganisms, such as bacteria and yeast, to multicellular organisms, such as animals and plants as well as humans with higher-order brain functions. Every single biological function is determined by the structure and dynamics of biological macromolecules such as proteins and nucleic acids and highly dynamic and complex networks of their interactions. The structures of biological macromolecules are defined by three-dimensional (3D) arrangements of so many component atoms, from a few thousands to tens and hundreds of thousands. Their structures are not solid like bulk materials of metals and ceramics but are very dynamic and flexible due to the network of weak non-covalent bonds that hold the 3D arrangement of component atoms. Their structures are designed to function by actively utilizing thermal fluctuations, and that is why the biological organisms can sustain their activities at an extremely low energy level compared to man-made machines. One of the major challenges in life science is the elucidation of mechanisms of complex biological functions based on the structures, dynamics and interactions of macromolecules involved in those functions, and it is therefore inevitable to look at the 3D structures of so many biological macromolecules and their stable or transient complexes in various states involved in various biological functions. The number of 3D structures we need to visualize would range from a few million to a few hundreds of millions or probably many more.

The 2017 Nobel Prize in Chemistry was awarded to three pioneers in the field of electron cryomicroscopy (cryoEM): Jacques Dubochet (University of Lausanne, Switzerland), Joachim Frank (Columbia University, USA) and Richard Henderson (MRC Laboratory of Molecular Biology, UK). The prize was awarded to them for their pioneering works in the development of cryoEM and image analysis for the structural analysis of macromolecules. Jacques Dubochet established a method of water vitrification by rapid cooling so that macromolecules can be embedded in the vitreous ice film to retain their native structures even in the vacuum of a transmission electron cryomicroscope (cryoTEM). Joachim Frank developed image processing algorisms to reconstruct 3D structures of macromolecules from their many two-dimensional (2D) projection images taken by TEM. Richard Henderson developed a method of electron crystallography and succeeded in reconstructing the 3D structure of a membrane protein 2D crystal at atomic resolution.

Received 26 October 2021; Revised 19 November 2021; Editorial Decision 20 November 2021; Accepted 21 December 2021

The 3D structures of macromolecules are the basic and essential information not only for life sciences but also for medical sciences and drug design. X-ray crystallography and NMR have been the two major techniques for high-resolution structural analysis of macromolecules over several decades, but the essential need of sample crystallization for X-ray crystallography and an upper limitation in the sample molecular mass of ∼50 kDa for NMR were the source of rather severe limitations to their much wider applications desired in many fields of life and medical sciences. CryoEM has become an extremely powerful tool for high-resolution structural analysis over the past several years and has now established its position as one of the essential techniques for structural analysis of macromolecules. CryoEM receives much attention because it can achieve near-atomic resolution or sometimes true atomic resolution in structural analysis of macromolecules from a very small amount of solution samples, as small as a few tens of micrograms or even a few micrograms in some cases, as far as they have well-defined 3D structures. No crystallization is needed, and there is virtually no upper limit in the molecular mass of specimens. The Nobel Prize was awarded to recognize the important contributions of the above three researchers as the founders of this technology. Here, we describe the concept of cryoEM single-particle image analysis as a technique for structural biology, history of progress and present state of technological development including our personal experiences, and the future potential of this technique for life and medical sciences through further development.

CryoEM single-particle image analysis of macromolecules

The powerful feature of cryoEM, especially single-particle image analysis, is that there is no need for sample crystallization that is essential for X-ray crystallography and that there is virtually no upper limit in the size of molecular complexes unlike NMR. Although determining the structures of small macromolecules <50 kDa is still a challenging task for cryoEM image analysis because they produce extremely low contrast in their ice-embedded state to be visible in cryoEM images, the other two techniques can be applied to them, and what we needed for structural life sciences is a method that allows us to look at so many macromolecular complexes in different functional states that are almost intractable by the other two techniques. However, since a large fraction of interatomic bonds that maintain their 3D structures are weak non-covalent bonds, such as hydrogen bonds, salt bridges and van der Waals contacts to produce hydrophobic interactions, the structures are very sensitive to electron beam irradiation damage, a few orders of magnitude worse than that of metals, ceramics and semiconductors. Therefore, to record high-resolution images of macromolecules and their complexes in their native, functional states without much damage, it is necessary to embed them in an amorphous ice thin film by rapidly freezing their aqueous solutions and record the images by a cryoTEM with a specimen stage cooled to a temperature below 100 K by liquid helium or liquid nitrogen to prevent the vitreous ice from converting to crystalline states. The lower the specimen temperature, the less the radiation damage [1], but at a temperature lower than 10 K–20 K, the low electron conductivity of ice and carbon on the specimen grid tends to cause image drift possibly by charging up [2]. Even at such low temperatures, the electron dose that can be irradiated without much damage to the atomic-level structures is limited to 20–30 e^{-} $Å^{-2}$. So, the quality of cryoEM images is extremely poor due to the intrinsic statistical noise, which is caused by a small number of electrons detected in each pixel of the image detector, as well as the Landau noise, which is a large distribution of signal levels of individual electron detected by the image detector. Since individual molecular images recorded by a cryoTEM are 2D projections of the 3D structure of molecules embedded in the amorphous ice film in various orientations, it is also necessary to collect a large number of images that are sufficient to cover different orientations with even distributions in order to reconstruct the 3D image at high resolution in every direction. So, it is essential to efficiently collect as many molecular images as possible, classify them into each orientation of projection and obtain averaged image for each orientation by aligning the position and orientation of the molecular images to increase the signal level while reducing the noise. This procedure is called 2D class average. Then, the relative relationships between the 2D class averaged images in the orientation of projection are determined, and finally, the 3D image of the molecule can be reconstructed (Fig. 1, adopted from [2]). To achieve high-resolution structural analysis, it is important to use a cryoTEM and an image detector both capable of efficiently collecting high-quality, high-resolution cryoEM images. High-precision image-analysis programs and high-speed computers are also required.

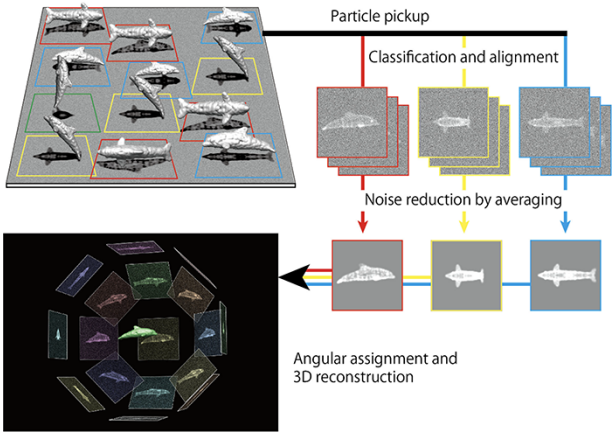

Fig. 1. Schematic diagram explaining the process of single-particle image analysis. Dolphins represent biological macromolecules embedded in a thin film of vitreous ice in various orientations. CryoEM images correspond to their 2D projections with high noise levels. After the S/N ratio is greatly increased by going through 2D classification and average of many 2D projections, a 3D image can be reconstructed by back projection. Adopted from [2].

CryoTEM with liquid helium stage and thermal field emission gun

To reduce the radiation damage as much as possible, Fujiyoshi *et al.* [3,4] designed and developed a cryoTEM with a very stable, liquid helium-cooled top-entry specimen stage to enable recording of high-quality cryoEM images of macromolecules.

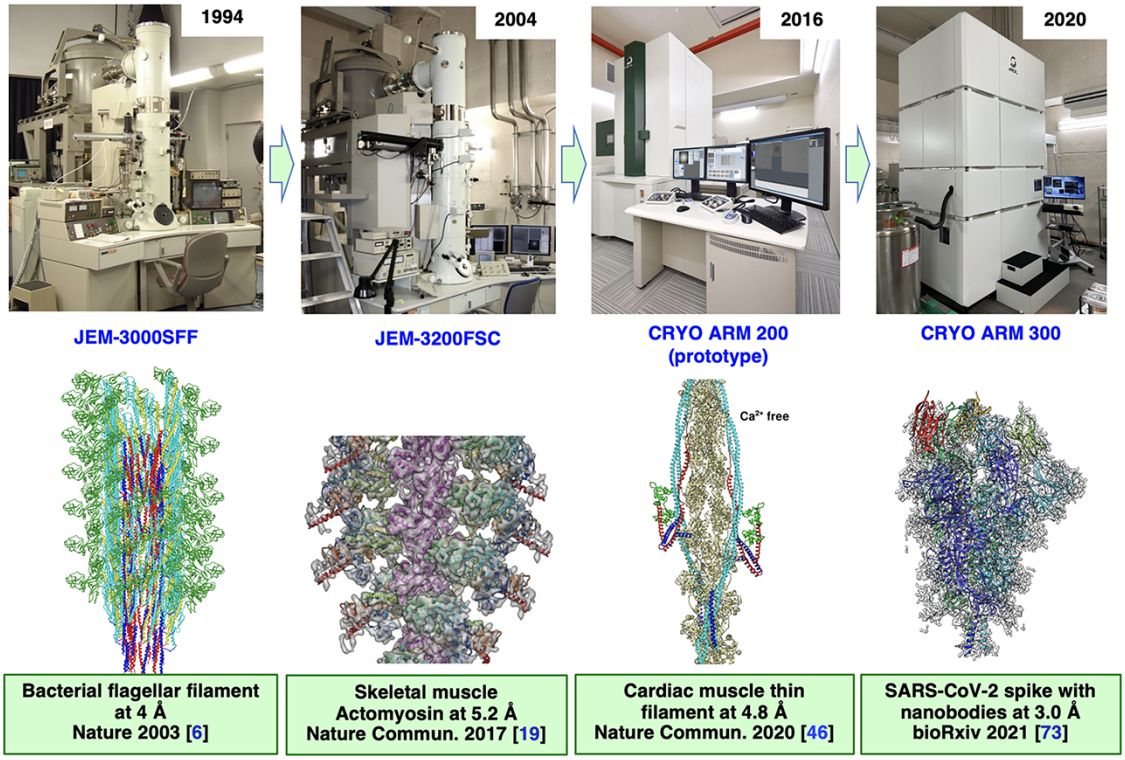

Fig. 2. Development history of cryoTEMs in our laboratory. From left to right: JEM-3000SFF with liquid He stage and thermal FEG; JEM-3200FSC with Ω-type energy filter and TVIPS F415mp CCD detector, in addition to liquid He stage and thermal FEG; CRYO ARM 200 prototype with liquid N_2 stage, cryo-grid autoloader, JADAS-based automated data collection and Gatan K2 CMOS detector, in addition to thermal FEG and Ω-type energy filter; CRYO ARM 300 with cold FEG, upgraded Ω-type energy filter, Gatan K3 detector and SerialEM-based high-throughput automated data collection, in addition to liquid N_2 stage, cryo-grid autoloader. Lower panels show the structures determined by the cryoTEMs above.

In early 1990s when Yoshinori Fujiyoshi and I started our new laboratories at the Panasonic Institute in Keihanna Science City, Kyoto, we requested JEOL to introduce a Schottky-type field emission electron gun (thermal FEG) to the liquid helium-cooled 300-kV cryoTEM (JEOL JEM-3000SFF) (Fig. 2). This was the very first cryoTEM with an FEG [2,4], and we expected a significant improvement in the quality and resolution of electron microscopy (EM) images by the high coherence of its electron beam by field emission. The improvement was remarkable with every cryoEM image showing up much stronger signals in high resolution [5–10]. Helical image analyses of a straight form of the bacterial flagellar filament and tubular crystals of the nicotinic acetylcholine receptor channel produced 3D density maps with their resolution high enough to allow atomic model building [6,7]. The 2D crystal structures of membrane proteins, such as bacteriorhodopsin and aquaporin, were solved at atomic resolution by electron crystallography combining imaging and diffraction [8–10]. However, because only photographic films were available as an image detector in those days, the efficiency and throughput of high-quality image data collection were extremely low. Therefore, it took more than several years for those structural analyses to reach near-atomic resolution, but many impactful results were produced and published in early to mid-2000s [6–10]. Our helical image analysis of the bacterial flagellar filament reached a resolution close to 4 Å from a small number of highly selected filament images containing only 40 000 flagellin molecules, where the polypeptide backbone and large side chains were resolved for the first time by cryoEM image analysis [6].

CCD detector and energy filter

Although the development of automated image data collection by charge coupled device (CCD) detectors was initiated in late 1990s [11–14], most of the labs continued to use photographic films through 2000s because the resolving power of CCD detectors was significantly lower than that of the film. The resolving power of CCD was lower because each electron forming an EM image had to be converted to photons by a thin layer of scintillator on top of the glass-fiber coupling block on the CCD chip, and the spot of each electron became blurred by electron scattering within the scintillator. However, the capability of image evaluation immediately after the exposure was a great advantage for efficient data collection. So, we started using a CCD detector in 2004 to improve the efficiency in high-quality data collection. We requested JEOL to equip the 300-kV liquid helium-cooled FEG cryoTEM with a 4k × 4k slow-scan CCD detector (TVIPS F415MP), together with an in-column Ω-type energy filter (JEOL JEM-3200 FSC) (Fig. 2) for our new laboratory at Osaka University. In those days, such CCD detector was still mostly used for electron diffraction recording. The Ω-type energy filter was introduced to improve the signal-to-noise (S/N) ratio of cryoEM images by removing a large portion of inelastically scattered electrons, which lost the coherence due to energy loss and

therefore contribute only to a high background noise and not to high-resolution EM images. This energy filter was the second generation designed by JEOL with an improved stability and handling capacity compared to the previous generation, and it was easy to use. We found nearly 2-fold improvement in the image S/N ratio just by this energy filter [15]. We used a relatively high magnification (∼90 000×) to compensate for the low resolving power of the CCD detector. The 4k × 4k CCD detector, albeit with the disadvantage in the resolving power, markedly improved the efficiency and throughput of high-quality image data collection because we were able to examine the EM image and its Fourier transform on the display monitor immediately after exposure, allowing us to make a quick and reliable judgment on the quality and resolution of individual cryoEM images during data collection [15]. We also improved the efficiency of high-quality image data collection further by elevating the specimen temperature from 4 K to ∼50 K by stopping the liquid helium flow from the in-column tank to the specimen pod. Although the radiation damage can be minimized at 4 K, most of the cryoEM images recorded at such low temperatures suffered from local image drift due to the charge up by electron irradiation because of the extremely poor electrical conductivity of the thin specimen ice film. It was less than a few percent of collected images that could be used for image analysis. Elevating the specimen temperature to ∼50 K made almost all the images to be sufficiently high quality to be used for image analysis [15].

These technological improvements and advances made previously multi-year projects to be completed within a couple of weeks from data collection to 3D reconstruction and allowed us to solve the structures of many different, interesting biomolecular assemblies, such as the bacterial flagellar hook and rod, muscle actin and actomyosin filaments, the ParM filament that segregates plasmids for bacterial cell division, the thin needle tube of the virulence type-III secretion system of pathogenic bacteria, all at 5–7 Å resolutions [15–20]. We were able to gain good insights into the mechanisms of their functions by docking and refining the available crystal structures of component proteins to the 3D maps to build their atomic models. The structure of the stacked disk formed by the tobacco mosaic virus coat protein was solved at 3.8 Å resolution also within a couple of weeks to allow many of the side chains to be visualized (Fujii *et al*., unpublished).

CMOS direct electron detector

The cryoEM field has been having a wonderful time since the arrival of a CMOS-based direct electron detector camera in 2013 [21]. David Agard and his colleagues at the University of California, San Francisco, had been developing an EM image detector in collaboration with Gatan, one of the major EM camera manufacturers, by repurposing a CMOS image sensor device for X-ray developed by a group at the University of California, Berkeley. Gatan completed this camera system as K2 Summit. This CMOS imaging chip had wonderful specifications: 4k × 4k pixels, robustness against irradiation of high-energy electrons of 300 keV or even higher; a minimal image blur by electron scattering within the very thin electron-detecting semiconductor layer; and best of all, a data acquisition rate of 400 frames per second, which made single-electron counting and movie-mode imaging possible. Because the total electron dose typically used for cryoEM image recording was $20 \sim 30$ e– Å^{-1} over 1 s, the number of electrons coming onto the detector plane in each frame could be made limited and countable if the dose rate was lowered enough by making the exposure time longer by ∼10-fold. Single-electron counting was quite effective in reducing the image noise level by minimizing the Landau noise, which is an intrinsic noise of detector with a large distribution of signal amplitude produced by each electron detection that any types of image sensor suffer [21]. Although a relatively large statistical noise still remains due to the small number of electrons used for a low-dose cryoEM imaging to avoid radiation damage, the improvement in image quality was significant.

Cheng and his colleagues thus made use of most of the high performance of this CMOS camera system and devised a way to collect sharp high-quality cryoEM images of macromolecules by movie-mode imaging and motion correction [21]. They successfully analyzed the 3D structures of a transmembrane protein, the TRPV1 receptor ion channel that senses heat and spiciness, which eluded crystallization over many years despite much effort. They solved the structures from a small amount of solution sample and published two papers in *Nature* [22,23]. The structure was solved at 3.3 Å resolution by analyzing ∼100 000 particle images of the detergent-solubilized membrane protein picked up from ∼1000 cryoEM images. After individual frame processing for single-electron counting, they added up every 80 frames to make a cryoEM movie of 5 frames per second and then added up these movie frames with motion correction to minimize the image blur caused by a mechanical drift of the specimen stage and the distortion of ice film caused by electron irradiation to make the final cryoEM image very sharp [21]. Since then, the highest resolution as well as average resolution of cryoEM structures have shown a steady improvement, partly due to the accuracy improvement in the image analysis software programs such as MotionCor2, CTFFIND4, gctf, RELION and cryoSPARC [24–29]. The high resolution record has been updated nearly every year as follows: 3.2 Å for β-galactosidase in 2014 [30], 2.6 Å for rotavirus in 2015 [31], 2.2 Å for β-galactosidase in 2015 [32], 1.8 Å for glutamate dehydrogenase in 2016 [33], 1.65 Å and 1.62 Å for apoferritin in 2018 [28,34], 1.53 Å for apoferritin in 2019 [35], and 1.25 Å and 1.22 Å for apoferritin [36,37].

Cold field emission gun and monochromator

Thermal FEG has played an important role in the improvement of resolution in cryoEM structural analysis over the past three decades because of its significantly higher coherence of the electron beam than that produced by conventional electron guns with a LaB_6 or W chip. The coherence of the electron beam is determined by the size of electron emission source on the chip as well as the energy spread. The size of the emission source of thermal FEG is 15–20 nm, and the energy spread of the electron beam accelerated to 300 keV is ∼0.7 eV. However, the recent achievements of the high-resolution apoferritin structures near 1 Å described above were made possible by further improvement in the coherence of electron beam produced either by cold FEG or monochromator with thermal FEG. Kato *et al*. [35] and Nakane *et al*. [37] used cryoTEMs with cold FEG that produces the electron beam emitted from a source size of 5–10 nm and with an energy spread of around 0.35 eV. Yip *et al*. used a cryoTEM

with a monochromator and a spherical-aberration corrector with thermal FEG to narrow the energy spread to 0.1 eV [36].

The 3D density maps of apoferritin at resolutions of 1.22 Å [37] and 1.25 Å [36] are both impressively showing the positions of hydrogen atoms as well as those of individual atoms of carbon, nitrogen and oxygen, demonstrating that cryoEM image analysis can achieve true atomic resolution as far as the structures of target macromolecules are stable enough. This is critical for understanding physical and chemical reaction mechanisms of proteins and making structure-based drug design more accurate and efficient. It is therefore encouraging that even current cryoTEM with a high-end detector will enable structures of macromolecular complexes to be determined at atomic resolution, and we can expect many more structures to be determined at atomic resolution. However, to achieve sub-Å resolution, a combination of these cutting-edge technologies, such as cryoTEM with cold FEG and monochromator, will be necessary.

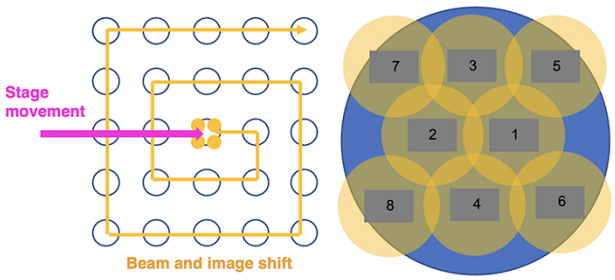

Fig. 3. Procedure of multi-hole/multi-shot imaging by beam tilt and image shift. Multi-hole imaging records images in surrounding holes (5 × 5 in this case) by beam tilt and image shift without stage movement in the order as indicated by the yellow arrow (left). In addition to this, multi-shot imaging records multiple images within each hole. In the case of zero-fringe mode (right), it is possible to take eight images within a single hole even with a 1.2 mm hole of the Quantifoil R1.2/1.3 holey carbon grid.

High-throughput data collection

The development of automated data collection systems was started in late 1990s [11–14], but the throughput was limited due to a relatively slow speed in image data acquisition by the slow-scan CCD detector used in those days. The FEI company (Thermo Fisher Scientific (TFS) since 2017) also started developing high-performance user-friendly cryoTEMs with a computer-controlled cryo-grid specimen stage and automatic grid loading device to make it easier for structural biologists to collect cryoEM images. FEI produced Titan Krios in 2008 as a particularly user-friendly cryoTEM, capable of storing 12 cryo-grids in a magazine and allowing users to load each grid onto the specimen stage by automatic loading device and to start automated data collection by specifying areas on the grid for image recording after grid quality judgment. Together with the arrival of CMOS direct electron detectors, such as Gatan K2 and K3 or TFS Falcons, Titan Krios became the most popular cryoTEM in the last several years because of its excellent capability of high-throughput data collection of high-resolution images. This highly automated cryoTEM also made 3D observation of cellular structures by electron cryotomography easier. However, the data collection throughput for single-particle image analysis was limited to around 1000–1500 images per day until 2018 [38], because every shot required a waiting time of several 10s of seconds after stage movement from one hole to the next for the specimen stage drift to become small enough for imaging, although the exposure and data acquisition time was only 10–15 s at most. Recently, however, multi-spot imaging using beam tilt and image shift became a standard practice to record images of 3 × 3 or 5 × 5 grid holes around the axis of electron optics without moving the stage, possibly with a multi-shot imaging within each hole (Fig. 3) [39–42]. The throughput markedly increased and reached 500 images per hour or 12 000 images per day (Fig. 4) without sacrificing high-resolution structural information to reach atomic resolution in 3D reconstruction [43,44].

In 2010, we requested JEOL to develop an automated cryoTEM based on the JEM-ARM200F they produced in 2009 as a high-resolution TEM for material research. Utilizing its ultra-high-resolution electron optics achieving sub-Å resolution imaging for a cryoTEM with the Ω-type in-column energy filter to minimize inelastically scattered electrons to increase the image S/N ratio and a highly stable computer-controlled liquid nitrogen-cooled specimen stage was thought to be an excellent choice to maximize the performance of its high-resolution electron optics for structural biology. We also asked for a cryoEM grid autoloader to be more user-friendly and convenient than that of Titan Krios. The Ω-filter is also useful for quickly measuring the thickness of ice film for grid quality judgment. A prototype of the new 200 kV cryoTEM named CRYO ARM arrived at our lab in the early summer of 2016 (Fig. 2). Although it took nearly a year to fix the bugs in mechanical hardware and software to control the automated grid loading device, once it started its stable operation in 2017 after all the hard work by JEOL engineers, the automated data collection system run by an improved and updated version of JADAS [14] as an automated data acquisition software allowed us to collect 2500 cryoEM image of β-galactosidase within 3 days, and the structure was reconstructed by RELION 2.0 [27] at 2.6 Å resolution (EMDB ID: 6840) [2], which was later refined to 2.4 Å. We were able to determine many biologically important structures with this cryoTEM, such as a native supercoiled flagellar hook [45], cardiac muscle thin filament in the presence and absence of Ca^{2+} [46], and flagellar LP ring as a bushing of the rotary motor [47]. Unfortunately, cold FEG was not equipped to this cryoTEM because it was not yet available at the time of initial design of this prototype CRYO ARM. But then, the commercial version of CRYO ARM 300 was equipped with cold FEG, and the first one was delivered to RIKEN SPring-8 Center in 2018. We used it to demonstrate the high-resolution imaging capability of this cryoTEM by reconstructing 1.53 Å apoferritin structure from ∼1000 images collected in 1 day [35] by using RELION 3.0 [28].

In collaboration with JEOL and with a funding support by the AMED CiCLE program, we then set to further improve the data collection throughput with a slightly updated version of CRYO ARM 300 installed at our laboratory in early 2020, with Gatan K3 detector, which runs at a frame rate of 1500 per second. With PyJEM, a python software library prepared by JEOL to control its TEM systems including the entire electron optics, specimen stage, cryogen refilling device and camera system, and based on SerialEM developed for automated data collection by TEM [48], a user-friendly workflow for grid screening, data acquisition area search and setting,

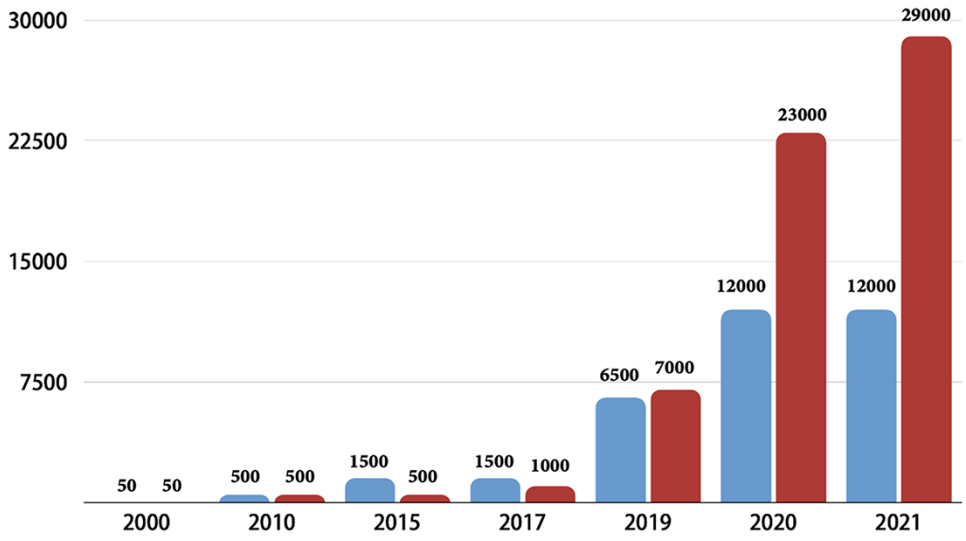

Year	CryoTEM	Detector	Data collection method
2000	JEM3000SFF	Photographic film	Manual
2010	JEM3200FSC	TVIPS F415mp	Manual
2017	CRYO ARM 200 (prototype)	GATAN K2	JADAS
2019	CRYO ARM 300	GATAN K3	SeraiEM
2020	CRYO ARM 300	GATAN K3	SerialEM & PyJEM
2021	CRYO ARM 300 II	GATAN K3	SerialEM & PyJEM & Zero-fringe

Fig. 4. History of improvement in cyroEM data collection throughput. The bar graphs show the maximum numbers of images that can be collected per day in each record update year indicated at the bottom. The blue bars represent the record by TFS cryoTEMs [38,39,41,42], and the red bars represent those by JEOL cryoTEMs in our laboratory. CryoTEMs, detectors and data collection methods used for data collection are listed in the bottom table [2,6,11]. The throughputs of 50 per day in 2000 and 500 per day in 2010 are rough estimates around those time.

and high-throughput data collection was established. With a multi-hole, multi-shot imaging scheme, the highest throughput was dramatically increased from 1000 per day in early 2019 to 1000 images per hour or 23 000 images per day in the summer of 2020 (Fig. 4). This advanced feature was very useful for quickly determining a multiple number of the bacterial flagellar rotor ring structures formed by full-length *Salmonella* FliF and its C-terminally truncated fragments [49]. With a fringe-free imaging by Köhler illumination that became available recently for CRYO ARM microscopes and with Gatan K3 as a detector, the throughput was further improved to 29 000 images per day (Fig. 4) [50]. Although this maximal speed can be used in routine data collection once the cryoTEM optics is well-calibrated, it should be noted that it requires a short exposure time of 0.5–1.0 s that can be used at a magnification higher than 100k, high-speed beam shift around 0.5 s or less achieved by using PyJEM, and recording over 100 images per stage movement.

Even in such high-throughput data collection, aberration-free image shift allows coma aberration caused by beam tilt to be minimized and high-resolution structural information to be kept free of phase error for 3D reconstruction to reach atomic resolution (Fig. 5). In our test data collection and analysis with apoferritin with CRYO ARM 300 and K3 detector, the structure was determined at 1.29 Å resolution from 7500 images collected in a 15-h session [50], but since the number of images of apoferritin generally required to reach 1.3 Å is less than half of this [43,44] and the throughput can be more than doubled easily, it would in principle be feasible to reach atomic resolution by a few hours of data collection.

Further improvements in electron optics and stability for higher resolution

It is remarkable to see the speed of recent improvements in cryoTEM hardware and software by TFS and JEOL toward highest possible resolution in macromolecular structural analysis at highest possible throughput in data collection, as clearly demonstrated by the multiple atomic resolution structures of apoferritin [36,37,43,44,51]. It seems to have become a routine for the apoferritin structure to be solved at atomic resolution. Now, although the anticipation of achieving sub-Å resolution is not at all far-fetched by a combination of cold FEG and monochromator, even the present high-end cryoTEMs with an excellent performance and stability of electron optics and specimen stage may give us a chance to go beyond 1 Å resolution.

One of the standard methods to examine the highest possible image resolution of a cryoTEM is to take an EM image of a test specimen, such as an amorphous platinum–iridium (Pt/Ir) thin alloy film, under a relatively large defocus condition of ∼1 μm, and look at its Fourier transform to see how far the Thon ring extends (Fig. 6). Frozen-hydrated

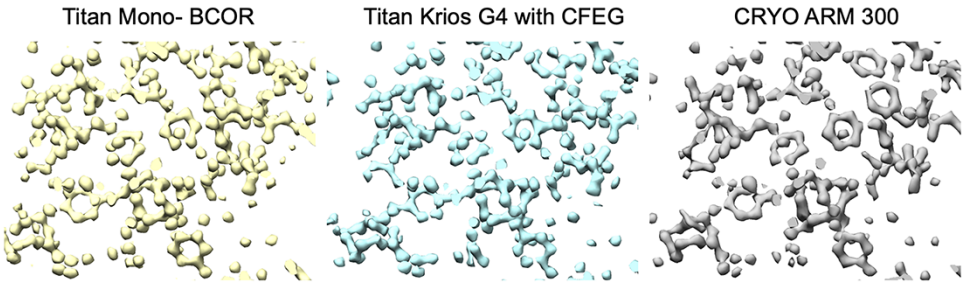

Data collection condition

CryoTEM	Titan Mono- BCOR	Titan Krios G4	CRYO ARM 300
Gun	FEG + Monochromator	Cold FEG	Cold FEG
Acceleration Voltage	300 kV	300 kV	300 kV
Magnification (pixel size)	- (0.492 Å/pix)	270,000x (0.457 Å/pix)	120,000x (0.437 Å/pix)
Detector	Falcon3	Falcon4	K3
Dose [$e^-/Å^2$]	50	40	40
Resolution [Å]	1.15	1.22	1.29
Number of images	10,398	3,370	7,500
Number of particles	797,000	363,126	527,261
Data collection speed [images/hour]	100	95	500

Fig. 5. Comparison of three cryoTEMs that achieved atomic resolution. The upper panels show part of the 3D density maps of apoferritin. The names of three cryoTEMs and data collection conditions are listed in the lower panel.

ice-embedded macromolecules need to be imaged by cryoTEM at such large defocuses to make them visible for image analysis by enhancing the low-resolution image contrast. By using a thin film of alloy, we are not limited by a low electron dose to avoid radiation damage so that we can examine how far the Thon ring signal extends to high resolution in the Fourier space. In the Fourier transform of Pt/Ir images taken by a 300 kV cryoTEM with thermal FEG (JEM-3200FSC), the Thon ring disappears beyond ∼1.8 Å resolution [52], but they extend to almost 1.1 Å by CRYO ARM 300 with cold FEG [2], clearly demonstrating the higher coherence of the electron beam. Interestingly, the Pt/Ir images taken by CRYO ARM 300 II show the Thon ring extending to 0.9 Å (Fig. 6), which is a significant improvement in resolution that was not really predicted by the hardware design. This could be due to a higher vacuum level around the cold FEG chip that may have made the size of emission source smaller and/or the higher stability in the accelerating voltage. In any case, this is quite encouraging for high-resolution structural analysis of macromolecules because the amplitude envelope of the phase contrast transfer function decays more slowly to maintain high-resolution image signals. It may be possible to reach a resolution close to 1.0 Å if every other high-resolution imaging condition is well fulfilled with this cryoTEM.

Prediction of further improvement in the throughput

Data collection throughput is determined mainly by four factors: exposure time, image data recording time, beam shift time and number of images recorded per stage movement by multi-hole/multi-shot imaging [53]. We can use the following equation to estimate the throughput as the number of images N collected per 24 h (86 400 s):

$$N = (86{,}400 - t_{LN}) / \left(t_{Stage}/n + t_{Img}\right),$$

where n is the number of images per stage movement, t_{LN} is the liquid nitrogen filling time per day, t_{Stage} is the total time of operations per stage movement including the time for stage shift, drift to settle and focusing and t_{Img} is the cumulative time of image recording including exposure, image data acquisition and beam shift. In the standard setting with our CRYO ARM 300, the exposure time for movie-mode imaging for a total dose of 40 $e^-/Å^{-2}$ is 0.5 s at a magnification of ×100k or 3.0 s at ×60k, the image data acquisition time is 2.0 s and the time for beam shift is 0.5 s, and therefore, t_{Img} is either 3.0 s or 5.5 s, t_{Stage} is 31 s and t_{LN} is 2400 s (20 min × 2). With these parameters, we can simulate how much further the data collection throughput could be improved by a shorter exposure time that can be achieved by a faster frame rate and a shorter data acquisition time that can be made possible by a CMOS sensor chip circuit design. If the data acquisition time is made as short as 0.5 s, the speed of data collection becomes over 50 000 images per day at a magnification of ×100k and 20 000 images per day at a magnification of ×60k (Fig. 7). It would become a routine session to collect data from around 10 different samples per day.

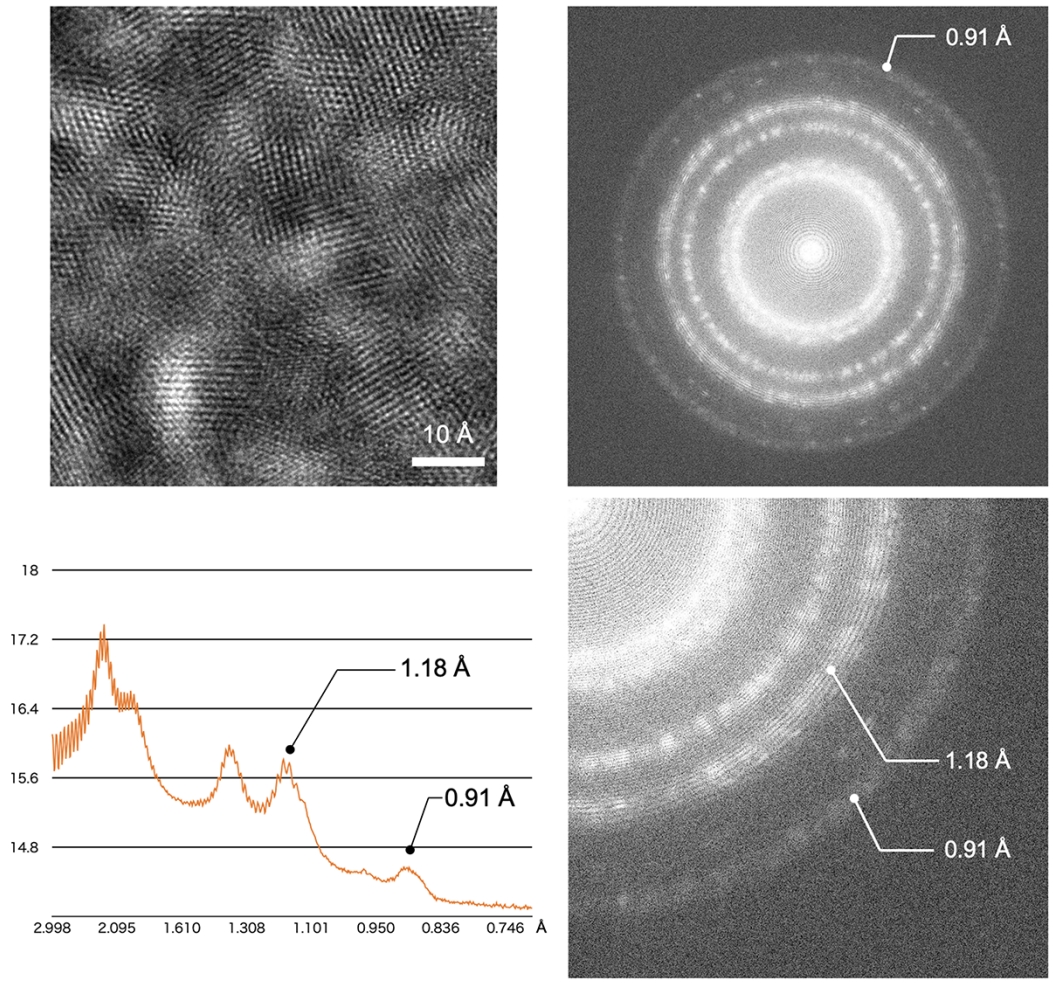

Condition for information limit of thon rings

CryoTEM	CRYO ARM 300 II	**Magnification (pix size)**	300k (0.17 Å/pix)
Acceleration voltage	300 kV	**Exposure time**	12 sec
Sample	Pt/Ir	**Dose (total)**	8 e-/pix/s (~6000 $e^-/Å^2$)
Camera	K3	**Defocus**	-1000 nm

Fig. 6. Evaluation of information limit of CRYO ARM 300 II by Thon rings of Pt/Ir. Upper left is a cryoEM image of Pt/Ir at 300k magnification. Upper right is the Fourier transform showing Thon rings extending to 0.91 Å. Lower left is one-dimensional profile of the Thon rings. High-resolution peaks at 1.18 Å and 0.91 Å are indicated. Lower right is a magnified image of upper right panel. Table at the bottom shows the parameters used for imaging.

Cryo-specimen grid preparation as the last bottleneck

Until a few years ago, the relatively low throughput of cryoEM imaging, taking a few days to collect a few thousands of images as a set of data, was one of the major bottlenecks in the macromolecular structural analysis by cryoEM image analysis. But the impressive improvement by beam-tilt/image-shift imaging as described above made the computation for image analysis to be a bottleneck. Now the last major bottleneck is cryo-specimen grid preparation. For efficient collection of high-quality cryoEM images for high-resolution structural analysis, macromolecular particles must be well dispersed in aqueous solution film of a few 10s-nm-thick within each hole of a holey carbon grid to be flash-frozen so that the particles can be embedded in thin vitreous ice film in various orientations [54]. Highly automated vitrification devices have been developed [55–58], and various efforts have been made to produce high-quality grids with well-dispersed particles without much sample loss by denaturation [55–61]. Macromolecules tend to localize to the air–water interface in a thin aqueous film and denature, leading to poor particle density and preferred orientation and making high-resolution 3D reconstruction inefficient [62]. Due to such problems, optimizing conditions for cryo-grid preparation requires much time and effort [63,64]. Thin support films such as graphene have been used to change the physical properties of grid surface to overcome these problems [65–68]. Graphene itself is not a good support due to its hydrophobicity, but it can be hydrophilized by conventional glow discharge or chemical modification [69]. Graphene oxide synthesized from graphite [70,71] can also be used as a hydrophilic derivative and is easy to obtain at low cost, but its small flaky shapes mostly <10 μm make it little difficult to prepare a fully and homogeneously covered graphene-support grid with it. Some efforts have also

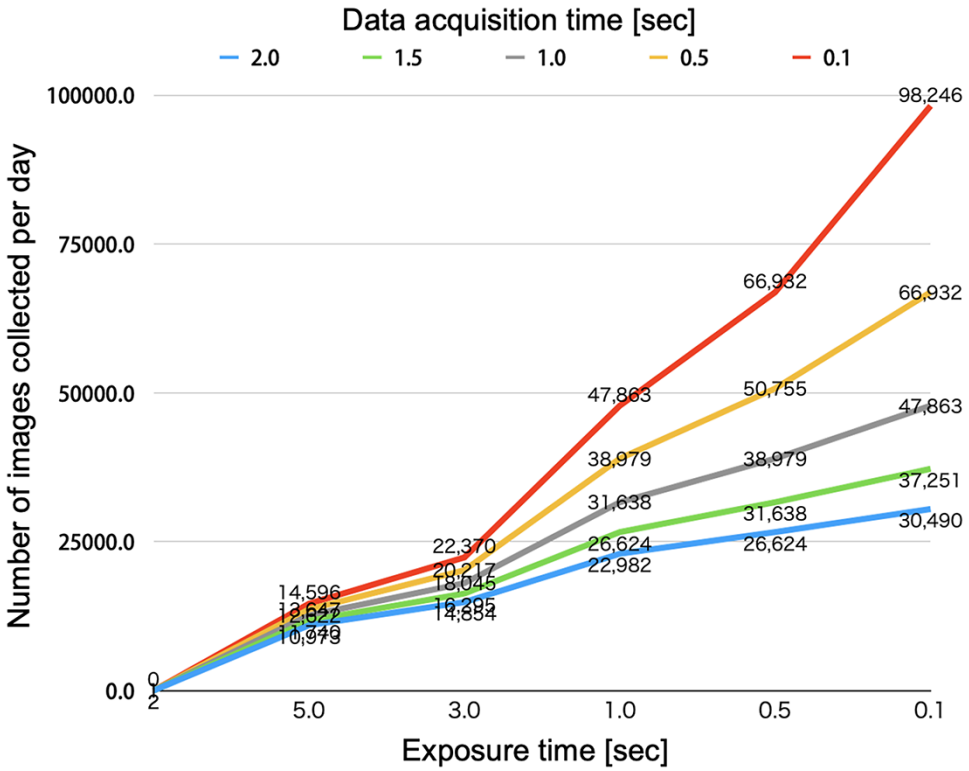

Fig. 7. Simulation of data collection throughput as images per day. Imaging condition parameters are set as follows according to those by Efremov and Stroobants [53]. The number of images recorded per stage movement is 200 by zero-fringe 5 × 5 × 8 multi-hole/multi-shot imaging. The liquid N_2 filling time is 40 min (20 min × 2) per day. The total operation time per stage movement before starting multi-hole/multi-shot imaging is 31 s, including stage shift, focusing and waiting time for drift to settle. The image recording time is the total time needed for taking one image, including the time for exposure, data acquisition, and beam-tilt and image-shift. The time for beam-tilt and image-shift is 0.5 s. Here, the exposure time and data acquisition time are the parameters for simulation.

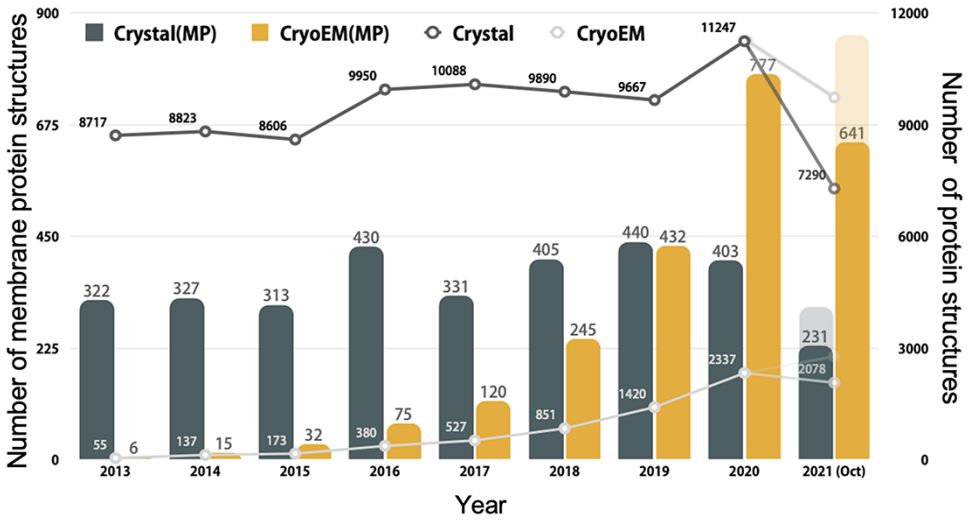

Fig. 8. Annual statistics on the number of structures deposited to the Protein Data Bank. The numbers are counted for structures with resolution better than 10 Å. Bar graphs represent those for membrane proteins (MP), and line plots are the total numbers of deposition per year by X-ray crystallography (crystal) and cryoEM (cryoEM). The numbers for 2021 are for those deposited by the end of September. Predicted 2021 full-year deposition numbers are shown in opaque lines and circles.

been made to utilize a large uniform sheet of graphene synthesized by chemical vapor deposition on metal substrates for cryoEM studies with additional surface functionalization [66,67]. Either non-specific or specific adsorption of macromolecules on the graphene support would keep most of macromolecules away from the air–water interface and could improve particle distribution and orientation.

We have developed an epoxidized graphene grid (EG-grid) that effectively immobilizes protein particles on the graphene surface by applying an oxidation reaction using

photoactivated $ClO_2^{\bullet}$ and further chemical modification [51]. This oxidation reaction introduces hydroxy groups onto a basal plane of graphene surface and then epoxy groups can be introduced by epichlorohydrin treatment, as has been used for functionalization of graphene oxide [72,73]. This EG-grid effectively immobilized proteins without tags. We tested this EG-grid for cryoEM structural analysis of GroEL, glyceraldehyde 3-phosphate dehydrogenase (GAPDH), β-galactosidase, apoferritin and severe acute respiratory syndrome coronavirus 2(SARS CoV 2) spike protein complexed with nanobodies. All of them showed high particle density and relatively homogeneous orientation, enabling effective data collection just by one or two grid preparation each. The resolutions of the final 3D maps of GroEL, GAPDH, β-galactosidase and apoferritin reached ∼2 Å or better. The resolution of apoferritin structure was 1.29 Å from 7500 images collected in 15 h, and the 2.0 Å structure of GroEL was obtained from only 504 images collected in 1 h. The protein concentration of the SARS-CoV-2 spike protein–nanobody complex solution applied on the EG-grid was only 0.1 mg ml^{-1}, but the resolution reached 3.03 Å from 4175 images [74], indicating a high particle density with less preferred orientation and denaturation by the adsorption to the epoxidized graphene for quick and efficient data collection for high-resolution structural analysis. By the development of more different types of supporting grids, such as the EG-grid cryo-grid preparation will soon become a quick routine procedure to make cryoEM structure determination an even more powerful tool for accelerating high-resolution structural analysis of macromolecules.

Trends in the number of data deposited to the protein data bank

After most of cryoEM structural analyses started to reach near-atomic resolution beyond 3 or 4 Å by the arrival of CMOS detectors in 2013, many atomic models have been built and the atomic coordinates deposited to the Protein Data Bank. While the annual deposition number of X-ray crystal data is nearly constant ∼10 000 in recent years, the number of cryoEM structure deposition has been increasing nearly exponentially since then, with ∼1.7-fold yearly increase in the last 5 years, to be over 2300 in 2020 (Fig. 8). Even a simple extrapolation of this exponential increase predicts the number of cryoEM data deposition to reach 11 500 in 2023, but considering the recent dramatic improvement in the data collection throughput as well as a steady increment in the computation speed by the development of computer hardware and image analysis software, it would be much sooner that cryoEM goes beyond X-ray crystallography to become the major technique for macromolecular structural analysis. For macromolecular complexes with molecular mass >500 kDa, the number of structures by cryoEM surpassed that of X-ray crystallography already a few years ago, and the number of membrane protein structures by cryoEM is already twice as many as that by X-ray in 2020 (Fig. 8).

Since all the functions and mechanisms that support life activities in living organisms are determined by the dynamic networks of biomolecules through their interactions, it is essential to elucidate the structures of the biomolecular complexes going through association and dissociation in atomic detail. Now, by recent advances in cryoEM techniques, the structures and intermolecular interactions have become increasingly visible for countless biomolecules that had previously been beyond our approach due to technical limitations, such as difficulty in crystallization or too large molecular size. The roles of cryoEM for the advancement of life sciences, medical sciences and drug design are immense. It is no exaggeration to say that the promotion of technological development in the cryoEM field to maximize its power is one of the most important issues for the future of human society.

Funding

Japan Society for the Promotion of Science KAKENHI Grant Number 25000013 to KN; Platform Project for Supporting Drug Discovery and Life Science Research (BINDS) from Japan Agency for Medical Research and Development under grant number JP19am0101117 to KN; the Cyclic Innovation for Clinical Empowerment (CiCLE) from AMED under grant number JP17pc0101020 to KN; JEOL YOKOGUSHI Research Alliance Laboratories of Osaka University to KN.

Acknowledgements

It is our honor to contribute this review article to the special issue of Microscopy commemorating its 70th anniversary. We thank Yoshinori Fujiyoshi, Takayuki Kato, Tomoko Miyata, Junso Fujita and so many engineers, staffs and managers at the headquarters and Osaka branch of JEOL, who have been helping us in our research studies in structural biophysics by technological development of cryoTEMs and its applications.

Conflict of interest

The authors declare that they have no conflict of interest.

References

1. Fujiyoshi Y, Uyeda N, Morikawa K, and Yamagishi H (1984) Electron microscopy of tRNA crystals II. 4 Å resolution diffraction pattern and substantial stability to radiation damage. *J. Mol. Biol.* 172: 347–354.
2. Namba K and Kato T (2018) Technical development of electron cryomicroscopy and contributions to life sciences. *JEOL News* 53: 18–24.
3. Fujiyoshi Y, Mizusaki T, Morikawa K, Yamagishi H, Aoki Y, Kihara H, and Harada Y (1991) Development of a superfluid helium stage for high-resolution electron microscopy. *Ultramicroscopy* 38: 241–251.
4. Fujiyoshi Y (2009) Observation of membrane proteins through an electron beam. *JEOL News* 44: 23–31.
5. Mimori Y, Yamashita I, Murata K, Fujiyoshi Y, Yonekura K, Toyoshima C, and Namba K (1995) The structure of the R-type straight flagellar filament of Salmonella at 9 Å resolution by electron cryomicroscopy. *J. Mol. Biol.* 249: 69–87.
6. Yonekura K, Maki-Yonekura S, and Namba K (2003) Complete atomic model of the bacterial flagellar filament by electron cryomicroscopy. *Nature* 424: 643–650.
7. Miyazawa A, Fujiyoshi Y, and Unwin N (2003) Structure and gating mechanism of the acetylcholine receptor pore. *Nature* 423: 949–955.

8. Kimura Y, Vassylyev D G, Miyazawa A, Kidera A, Matsushima M, Mitsuoka K, Murata K, Hirai T, and Fujiyoshi Y (1997) Surface of bacteriorhodopsin revealed by high-resolution electron crystallography. *Nature* 389: 206–211.
9. Murata K, Mitsuoka K, Hirai T, Walz T, Agre P, Heymann J B, Engel A, and Fujiyoshi Y (2000) Structural determinants of water permeation through aquaporin-1. *Nature* 407: 599–605.
10. Gonen T, Cheng Y, Sliz P, Hiroaki Y, Fujiyoshi Y, Harrison S C, and Walz T (2005) Lipid-protein interactions in double-layered two-dimensional AQP0 crystals. *Nature* 438: 633–638.
11. Carragher B, Kisseberth N, Kriegman D, Milligan R A, Potter C S, Pulokas J, and Reilein A (2000) Leginon: an automated system for acquisition of images from citreous ice specimens. *J. Struct. Biol.* 132: 33–45.
12. Suloway C, Pulokas J, Fellmann D, Cheng A, Guerra F, Quispe J, Stagg S, Potter C S, and Carragher B (2005) Automated molecular microscopy: the new Leginon system. *J. Struct. Biol.* 151: 41–60.
13. Mastronarde D N (2005) Automated electron microscope tomography using robust prediction of specimen movements. *J. Struct. Biol.* 152: 36–51.
14. Zhang J, Nakamura N, Shimizu Y, Liang N, Liu X, Jakana J, Marsh M P, Booth C R, Shinkawa T, Nakata M, and Chiu W (2009) JADAS: a customizable automated data acquisition system and its application to ice-embedded single particles. *J. Struct. Biol.* 165: 1–9.
15. Fujii T, Kato T, and Namba K (2009) Specific arrangement of α-helical coiled coils in the core domain of the bacterial flagellar hook for the universal joint function. *Structure* 17: 1485–1493.
16. Fujii T, Iwane A H, Yanagida T, and Namba K (2010) Direct visualization of secondary structures of F-actin by electron cryomicroscopy. *Nature* **467**: 724–728.
17. Gayathri P, Fujii T, Møller-Jensen J, van den Ent F, Namba K, and Löwe J (2012) A bipolar spindle of antiparallel ParM filaments drives bacterial plasmid segregation. *Science* 338: 1334–1337.
18. Fujii T, Cheung M, Blanco A, Kato T, Blocker A J, and Namba K (2012) Structure of a type III secretion needle at 7-Å resolution provides insights into its assembly and signaling mechanisms. *Proc. Natl. Acad. Sci. USA* 109: 4461–4466.
19. Fujii T and Namba K (2017) Structure of actomyosin rigour complex at 5.2 Å resolution and insights into the ATP cycle mechanism. *Nature Commun.* 8: 13969.
20. Fujii T, Kato T, Hiraoka K D, Miyata T, Minamino T, Chevance F F V, Hughes K T, and Namba K (2017) Identical folds used for distinct mechanical functions of the bacterial flagellar rod and hook. *Nature Commun.* 8: 14276.
21. Li X, Mooney P, Zheng S, Booth C R, Braunfeld M B, Gubbens S, Agard D A, and Cheng Y (2013) Electron counting and beam-induced motion correction enable near-atomic-resolution single-particle cryo-EM. *Nat. Methods* 10: 584–590.
22. Liao M, Cao E, Julius D, and Cheng Y (2013) Structure of the TRPV1 ion channel determined by electron cryo-microscopy. *Nature* 504: 107–112.
23. Cao E, Liao M, Cheng Y, and Julius D (2013) TRPV1 structures in distinct conformations reveal activation mechanisms. *Nature* 504: 113–118.
24. Zheng S Q, Palovcak E, Armache J-P, Verba K A, Cheng Y, and Agard D (2017) MotionCor2: anisotropic correction of beam-induced motion for improved cryo-electron microscopy. *Nat. Methods* 14: 331–332.
25. Rohou A and Grigorieff N (2016) CTFFIND4: fast and accurate defocus estimation from electron micrographs. *J. Struct. Biol.* 193: 1–12.
26. Zhang K (2016) Gctf: real-time CTF determination and correction. *J. Struct. Biol.* 193: 1–12.
27. Kimanius D, Forsberg B O, Scheres S H W, and Lindahl E (2016) Accelerated cryo-EM structure determination with parallelization using GPUs in RELION-2. *eLife* 5: e18722.
28. Zivanov J, Nakane T, Forsberg B O, Kimanius D, Hagen W J H, Lindahl E, and Scheres S H W (2018) New tools for automated high-resolution cryo-EM structure determination in RELION-3. *eLife* 7: e42166.
29. Punjani A, Rubinstein J L, Fleet D J, and Brubaker M A (2017) cryoSPARC: algorithms for rapid unsupervised cryo-EM structure determination. *Nat. Methods* 14: 290–296.
30. Bartesaghi A, Matthies D, Banerjee S, Merk A, and Subramaniam S (2014) Structure of β-galactosidase at 3.2-Å resolution obtained by cryo-electron microscopy. *Proc. Natl. Acad. Sci. USA* 111: 11709–11714.
31. Grant T and Grigorieff N (2015) Measuring the optimal exposure for single particle cryo-EM using a 2.6 Å reconstruction of rotavirus VP6. *eLife* 4: e06980.
32. Bartesaghi A, Merk A, Banerjee S, Matthies D, Wu X, Milne J L S, and Subramaniam S (2015) 2.2 Å resolution cryo-EM structure of β-galactosidase in complex with a cell-permeant inhibitor. *Science* 348: 1147–1151.
33. Merk A, Bartesaghi A, Banerjee S, Falconieri V, Rao P, Davis M I, Pragani R, Boxer M B, Earl L A, Milne J L S, and Subramaniam S (2016) Breaking cryo-EM resolution barriers to facilitate drug discovery. *Cell* 165: 1–10.
34. Danev R, Yanagisawa H, and Kikkawa M (2018) Cryo-electron microscopy methodology: current aspects and future directions. *Trends Biochem. Sci.* 44: 837–848.
35. Kato T, Makino F, Nakane T, Terahara N, Kaneko T, Shimizu Y, Motoki S, Ishikawa I, Yonekura K, and Namba K (2019) CryoTEM with a cold field emission gun that moves structural biology into a new stage. *Microsc. Microanal.* 25: 998–999.
36. Yip K M, Fischer N, Paknia E, Chari A, and Stark H (2020) Atomic-resolution protein structure determination by cryo-EM. *Nature* 587: 157–161.
37. Nakane T, Kotecha A, Sente A, McMullan G, Masiulis S, Brown P M G E, Grigoras I T, Malinauskaite L, Malinauskas T, Miehling J, Uchanske T, Yu L, Karia D, Pechnokova E V, de Jong E, Keizer J, Bischoff M, McCormack J, Tiemeijer P, Hardwick S W, Chirgadze D Y, Murshudov G, Aricescu A R, and Scheres S H W (2020) Single-particle cryo-EM at atomic resolution. *Nature* 587: 152–156.
38. Baldwin P R, Tan Y Z, Eng E T, Rice W J, Noble A J, Negro C J, Cianfrocco M A, Potter C S, and Carragher B (2018) Big data in cryoEM: automated collection, processing and accessibility of EM data. *Curr. Opin. Microbiol.* 43: 1–8.
39. Weis F and Hagen W J H (2020) Combining high throughput and high quality for cryo-electron microscopy data collection. *Acta Cryst.* D**76**: 724–728.
40. Cheng A, Eng E T, Alink L, Rice W J, Jordan K D, Kim L Y, Potter C S, and Carragher B (2018) High resolution single particle cryo-electron microscopy using beam-image shift. *J. Struct. Biol.* 204: 270–275.
41. Wu C, Huang X, Cheng J, Zhu D, and Zhang X (2019) High-quality, high-throughput cryo-electron microscopy data collection via beam tilt and astigmatism-free beam-image shift. *J. Struct. Biol.* 208: 107396.
42. Li Y, Cash J N, Tesmer J J G, and Cianfrocco M A (2020) High-throughput cryo-EM enabled by user-free preprocessing routines. *Structure* 28: 858–869.
43. Zhang K, Pintilie G D, Li S, Schmid M F, and Chiu W (2020) Resolving individual atoms of protein complex by cryo-electron microscopy. *Cell Res.* 30: 1136–1139.
44. Danev R, Yanagisawa H, and Kikkawa M (2021) Cryo-EM performance testing of hardware and data acquisition strategies. *Microscopy* 2021: 1–11.
45. Kato T, Makino F, Miyata T, Horváth P, and Namba K (2019) Structure of the native supercoiled flagellar hook as a universal joint. *Nat. Commun.* 10: 5295.

46. Yamada Y, Namba K, and Fujii T (2020) Cardiac muscle thin filament structures reveal calcium regulatory mechanism. *Nat. Commun.* 11: 153.
47. Yamaguchi T, Makino F, Miyata T, Minamino T, Kato T, and Namba K (2021) Structure of the molecular bushing of the bacterial flagellar motor. *Nat. Commun.* 12: 4469.
48. Schob M, Haberbosch I, Hagen W J H, Schwab Y, and Mastronarde D N (2019) Software tools for automated transmission electron microscopy. *Nat. Methods* 16: 471–477.
49. Kawamoto A, Miyata T, Makino F, Kinoshita M, Minamino T, Imada K, Kato T, and Namba K (2021) Native flagellar MS ring is formed by 34 subunits with 23-fold and 11-fold subsymmetries. *Nat. Commun.* 12: 4223.
50. Oosaki A, Hosogi N, Makino F, Motoki S, Ishikawa I, Ookura Y, and Kobayashi K (2021) Development of high throughput cryo electron microscope with cold field emission gun (CRYO ARM^{TM} 300II). *Microsc. Microanal.* 30: 1634–1636.
51. Fujita J, Makino F, Asahara H, Moriguchi M, Kumano S, Anzai I, Kishikawa J, Matsuura Y, Kato T, Namba K, and Inoue T (2021) Epoxidized graphene grid for high-throughput high-resolution cryoEM structural analysis. *bioRxiv*. https://biorxiv.org/cgi/content/short/2021.11.17.468963v1.
52. Hamaguchi T, Maki-Yonekura S, Naitow H, Matsuura Y, Ishikawa T, and Yonekura K (2019) A new cryo-EM system for single particle analysis. *J. Struct. Biol.* 207: 40–48.
53. Efremov R G and Stroobants A (2021) Coma-corrected rapid single-particle cryo-EM data collection on the CRYO ARM 300. *Acta Cryst.* D77: 555–564.
54. Dubochet J, Adrian M, Chang J 0 J, Homo J-C, Lepault J, McDowall A W, and Schultz P (1988) Cryo-electron microscopy of vitrified specimens. *Q. Rev. Biophys.* 21: 129–228.
55. Jain T, Sheehan P, Crum J, Carragher B, and Potter C S (2012) Spotiton: a prototype for an integrated inkjet dispense and vitrification system for cryo-TEM. *J. Struct. Biol.* 179: 68–75.
56. Razinkov I, Dandey V P, Wei H, Zhang Z, Melnekoff D, Rice W J, Wigge C, Potter C S, and Carragher B (2016) A new method for vitrifying samples for cryoEM. *J. Struct. Biol.* 195: 190–198.
57. Dandey V P, Wei H, Zhang Z, Tan Y Z, Acharya P, Eng E T, Rice W J, Kahn P A, Potter C S, and Carragher B (2018) Spotiton: new features and applications. *J. Struct. Biol.* 202: 161–169.
58. Ravelli R B G, Nijpels F J T, Henderikx R J M, Weissenberger G, Thewessem S, Gijsbers A, Beulen B W A M M, López-Iglesias C, and Peters P J (2020) Cryo-EM structures from sub-nl volumes using pin-printing and jet vitrification. *Nat. Commun.* 11: 2563.
59. Lee J, Saha A, Pancera S M, Kempter A, Rieger J, Bose A, and Tripathi A (2012) Shear free and blotless cryo-TEM imaging: a new method for probing early evolution of nanostructures. *Langmuir* 28: 4043–4046.
60. Arnold S A, Albiez S, Bieri A, Syntychaki A, Adaixo R, McLeod R A, Gokdie K N, Stahlberg H, and Braun T (2017) Blotting-free and lossless cryo-electron microscopy grid preparation from nanoliter-sized protein samples and single-cell extracts. *J. Struct. Biol.* 197: 220–226.
61. Feng X, Fu Z, Kaledhonkar S, Jia Y, Shar B, Jin A, Liu Z, Sun M, Chen B, Grassucci R A, Ren Y, Jiang H, Frank J, and Lin Q (2017) A fast and effective microfluidic spraying-plunging method for high-resolution single-particle cryo-EM. *Structure* 25: 663–670.
62. D'Imprima E, Floris D, Jope M, Sánchez R, Grininger M, and Kühlbrandt W (2019) Protein denaturation at the air-water interface and how to prevent it. *eLife* 8: e42747.
63. Drulyte I, Johnson R M, Hesketh E L, Hurdiss D L, Scarff C A, Porav S A, Ranson N A, Muench S P, and Thompson R F (2018) Approaches to altering particle distributions in cryo-electron microscopy sample preparation. *Acta Cryst.* D**74**: 560–571.
64. Glaeser R M (2016) How good can cryo-EM become? *Nat. Methods* 13: 28–32.
65. Grassucci R A, Taylor D J, and Frank J (2007) Preparation of macromolecular complexes for cryo-electron microscopy. *Nat. Protoc.* 2: 3239–3246.
66. Han Y, Fan X, Sang H, Zhao F, Tully C G, Kong J, Yao N, and Yan N (2020) High-yield monolayer graphene grids for near-atomic resolution cryoelectron microscopy. *Proc. Natl. Acad. Sci. USA* 117: 1009–1014.
67. Naydenova K, Peet M J, and Russo C J (2019) Multifunctional graphene supports for electron cryomicroscopy. *Proc. Natl. Acad. Sci. USA* 116: 11718–11724.
68. Pantelic R S, Suk J W, Magnuson C W, Meyer J C, Wachsmuth P, Kaiser U, Ruoff R S, and Stahlberg H (2011) Graphene: substrate preparation and introduction. *J. Struct. Biol.* 174: 234–238.
69. Russo C J and Passmore L A (2014) Controlling protein adsorption on graphene for cryo-EM using low-energy hydrogen plasmas. *Nat. Methods* 11: 649–652.
70. Santamaría-Juárez G, Gómez-Barojas E, Quiroga-González E, Sánchez-Mora E, Quintana-Ruiz M, and Santamaría-Juárez J D (2019) Safer modified Hummers' method for the synthesis of graphene oxide with high quality and high yield. *Mater. Res. Express* 6: 125631.
71. Hummers W S and Offeman R E (1958) Preparation of graphitic oxide. *J. Am. Chem. Soc.* 80: 1339.
72. Hota P, Miah M, Gupta A, Chakravoty D, and Saha S K (2019) Epichlorohydrin functionalized graphene oxide for superior Li^{+} ion conduction and supercapacitor application. *Mater. Chem. Phys.* 223: 447–455.
73. Liu J-W, Yang T, Chen S, Chen X-W, and Wang J-H (2013) Nickel chelating functionalization of graphene composite for metal affinity membrane isolation of lysozyme. *J. Mater. Chem. B* 1: 810–818.
74. Maeda R, Fujita J, Konishi Y, Kazuma Y, Yamazaki H, Anzai I, Yamaguchi K, Kasai K, Nagata K, Yamaoka Y, Miyakawa K, Ryo A, Shirakawa K, Makino F, Matsuura Y, Inoue T, Imura A, Namba K, and Takaori-Kondo A (2021) Nanobodies recognizing conserved hidden clefts of all SARS-CoV-2 spike variants. *bioRxiv*